J. Mech. Phys. Solids 150 (2021) 104365

Contents lists available at ScienceDirect

Journal of the Mechanics and Physics of Solids

journal homepage: www.elsevier.com/locate/jmps

# Breakdown of continuum models for spherical probe adhesion tests on micropatterned surfaces

Simon Bettscheider [a,b], Dan Yu [a], Kimberly L. Foster [c,d], Robert M. McMeeking [a,c,e,f], Eduard Arzt [a,b], René Hensel [a], Jamie A. Booth [c,g,*]

[a] *INM – Leibniz Institute for New Materials, Campus D2 2, 66123 Saarbrücken, Germany*
[b] *Department of Materials Science and Engineering, Saarland University, Saarbrücken, Germany*
[c] *Mechanical Engineering Department, University of California, Santa Barbara CA 93106, USA*
[d] *School of Science and Engineering, Tulane University, New Orleans LA 70118, USA*
[e] *Materials Department, University of California, Santa Barbara CA 93106, USA*
[f] *School of Engineering, University of Aberdeen, King's College, Aberdeen AB24 3UE, UK*
[g] *Mechanical Engineering Department, California State University, Northridge CA 91330, USA*

ARTICLE INFO

*Keywords:*
Adhesion and adhesives (A)
Contact mechanics (B)
Mechanical testing (C)

ABSTRACT

The adhesion of fibrillar dry adhesives, mimicking nature's principles of contact splitting, is commonly characterized by using axisymmetric probes having either a flat punch or spherical geometry. When using spherical probes, the adhesive pull-off force measured depends strongly on the compressive preload applied when making contact and on the geometry of the probe. Together, these effects complicate comparisons of the adhesive performance of micropatterned surfaces measured in different experiments. In this work we explore these issues, extending previous theoretical treatments of this problem by considering a fully compliant backing layer with an array of discrete elastic fibrils on its surface. We compare the results of the semi-analytical model presented to existing continuum theories, particularly with respect to determining a measurement system- and procedure-independent metric for the local adhesive strength of the fibrils from the global pull-off force. It is found that the discrete nature of the interface plays a dominant role across a broad range of relevant system parameters. Accordingly, a convenient tool for simulation of a discrete array is provided. An experimental procedure is recommended for use in conjunction with this tool in order to extract a value for the local adhesive strength of the fibrils, which is independent of the other system properties (probe radius, backing layer thickness, and preload) and thus is suitable for comparison across experimental studies.

## 1. Introduction

Micropatterned dry adhesives have been shown to overcome current limitations in industrial handling operations (Hensel et al., 2018), demonstrating the ability to function in vacuum where suction can no longer be utilized and to grasp miniaturized objects such as surface mounted devices (SMDs) (Barreau et al., 2017; Mengüç et al., 2012; Minsky and Turner, 2017; Tinnemann et al., 2019a, 2019b).

* Corresponding author at: Mechanical Engineering Department, California State University, Northridge CA 91330, USA.
*E-mail address:* jamie.booth@csun.edu (J.A. Booth).

https://doi.org/10.1016/j.jmps.2021.104365
Received 9 October 2020; Received in revised form 21 January 2021; Accepted 9 February 2021
Available online 12 February 2021

In order to evaluate the adhesive performance of micropatterned adhesives, the use of axisymmetric probes has been widely favored (Cheung and Sitti, 2009; Greiner et al., 2007; Khaled and Sameoto, 2013; Yu et al., 2018). The intrinsic stiffness of the probe is typically much larger than the adhesive. In experiments, the probe approaches the adhesive surface until a specified compressive preload or indentation depth is reached. It is then retracted until both bodies separate. The load and displacement are simultaneously recorded throughout. The maximum value of the tensile load is defined as the 'pull-off' force, although this is strictly only the point of unstable detachment in a load-controlled measurement. This value can still be obtained in a displacement-controlled measurement, with the distinction being that stable attachment is maintained beyond this point until the surfaces are fully separated and the load drops to zero.

The challenge is to use the pull-off force to obtain an objective measure of adhesive strength, capturing the effects of the geometry of the surface microstructures and the character of the interface at the junctions formed but independent of the characteristics of the measurement system and procedure. This is required to allow for the comparison of performance across experimental investigations.

Flat-ended cylindrical probes are challenging to align to the surface of the sample, and alignment imperfections can cause a significant reduction in the detachment force (Bacca et al., 2016; Booth et al., 2018). In addition to probe geometry, the compliance of the backing layer on which the microstructures are fabricated also results in a characteristic contact edge load concentration (Bacca et al., 2016; Long et al., 2008), which complicates determination of an objective measure of the adhesive strength of the microstructures. The issue of misalignment can be alleviated through use of a spherical probe. However, several complications remain. These are the focus of this work.

Fig. 1 shows the pull-off force and strength as a function of preload for a fibrillar micropatterned adhesive tested using a spherical probe, as described in Section 2.3 and in the Supplementary Information (SI). The results of these experiments highlight the primary difficulties of obtaining an objective measure of strength using a spherical probe. Firstly, it is observed that the pull-off force depends on the preload, $P$, and on the radius of the spherical probe, $R$, as has been highlighted in previous work (Greiner et al., 2009, 2007; Kroner et al., 2011). As Greiner et al. (2007) warn, this "dependence can obscure comparison of the adhesion data obtained by different groups, as measurements are usually performed with different indenter geometries and at different preloads".

Several attempts have been made to theoretically describe the dependence of adhesive performance on the preload and probe radius. Schargott et al. (2006) present a model which addresses the limit of a rigid backing layer, treating the fibrils as a continuous layer of linear elastic springs which sit between spherical and nominally flat surfaces. This result was rederived in terms of the parameters used in this study in the SI. By prescribing the elastic response and defining the detachment force of an individual fibril, it is demonstrated that the pull-off force for the sample initially increases with increasing preload before saturating, as

$$F_{\text{pull-off}} = F_{\max}\begin{cases} 2\sqrt{\dfrac{P}{F_{\max}}} - \dfrac{P}{F_{\max}} & \text{for } \dfrac{P}{F_{\max}} < 1 \\ 1 & \text{for } \dfrac{P}{F_{\max}} \geq 1 \end{cases} \tag{1}$$

where $P$ is the preload applied when making contact, and $F_{\max}$ the maximum value of the pull-off force (i.e. measured in the saturation regime, as shown below). The maximum pull-off force can be stated in terms of the properties of the adhesive and probe as

$$F_{\max} = 2\pi R\left(\frac{\rho {f_{\max}}^2 h}{2\pi c^2 E}\right), \tag{2}$$

where $R$ is the radius of the probe, $\rho$ the areal density of fibrils, $f_{\max}$ the detachment force for an individual fibril, $h$ the fibril length, $c$ the fibril radius, and $E$ the Young's modulus of the fibril material. It is observed that the preload required to achieve saturation of the pull-off force is equal to the pull-off force itself in the saturation regime. This saturation behavior is apparent in the experimental

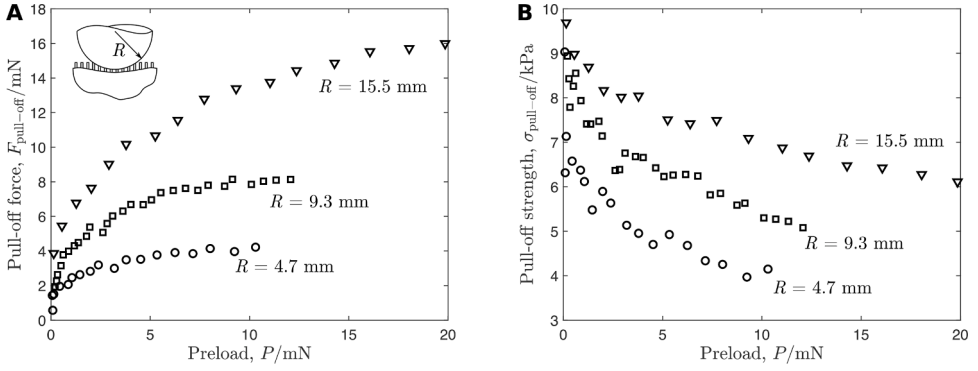


**Fig. 1.** (A) The pull-off force and (B) the pull-off strength as a function of preload. Spherical probes with radii of 4.7, 9.3 and 15.5 mm, indent a fibrillar adhesive. The fibrils have 25 μm radius, 100 μm length, and are arranged in a hexagonal pattern with a spacing of 100 μm. The experiment is described in Section 2.3 and in the Supplementary Information (SI).

results of Fig. 1. Upon measurement of the detachment force in the saturation regime, $F_{\text{pull-off}} = F_{\max}$, the result of equation ( 1 ) can be used to determine the detachment force of an individual fibril, $f_{\max}$. If the assumptions upon which the model is based hold for the experiment in question, namely that the backing layer can be considered rigid and the fibril layer continuous, then the detachment force of a fibril obtained using this method represents an objective measurement of the adhesive strength of the micropatterned surface.

An alternative approach is to utilize continuum theories of adhesion, assuming that the fibril layer is a feature of the interface and adopting an effective work of adhesion, which assumes that the strain energy in a fibril at detachment is not available to drive detachment of neighbors, and thus is lost in the separation process (Jagota, 2002). This leads to

$$W_{\text{eff}} = \frac{\rho {f_{\max}}^2 h}{2\pi c^2 E}. \tag{3}$$

When the backing layer is considered as rigid, the spherical probe adhesion test is consistent with the assumptions of the Derjaguin-Muller-Toporov (DMT) continuum theory (Derjaguin et al., 1975). The associated maximum pull-off force is

$$F_{\max} = 2\pi R W_{\text{eff}}. \tag{4}$$

It is identified that the result of the Schargott model for a rigid backing layer given in Eq. (2), when combined with the effective work of adhesion of Eq. (3), is consistent with this result. This is unsurprising given that it is based upon a continuous adhesive layer confined between a rigid sphere and nominally flat rigid surface.

One possibility for consideration of the backing layer compliance is to adopt another continuum theory, namely that of Johnson, Kendall, and Roberts (JKR) (Johnson et al., 1971), where the detachment force is given by

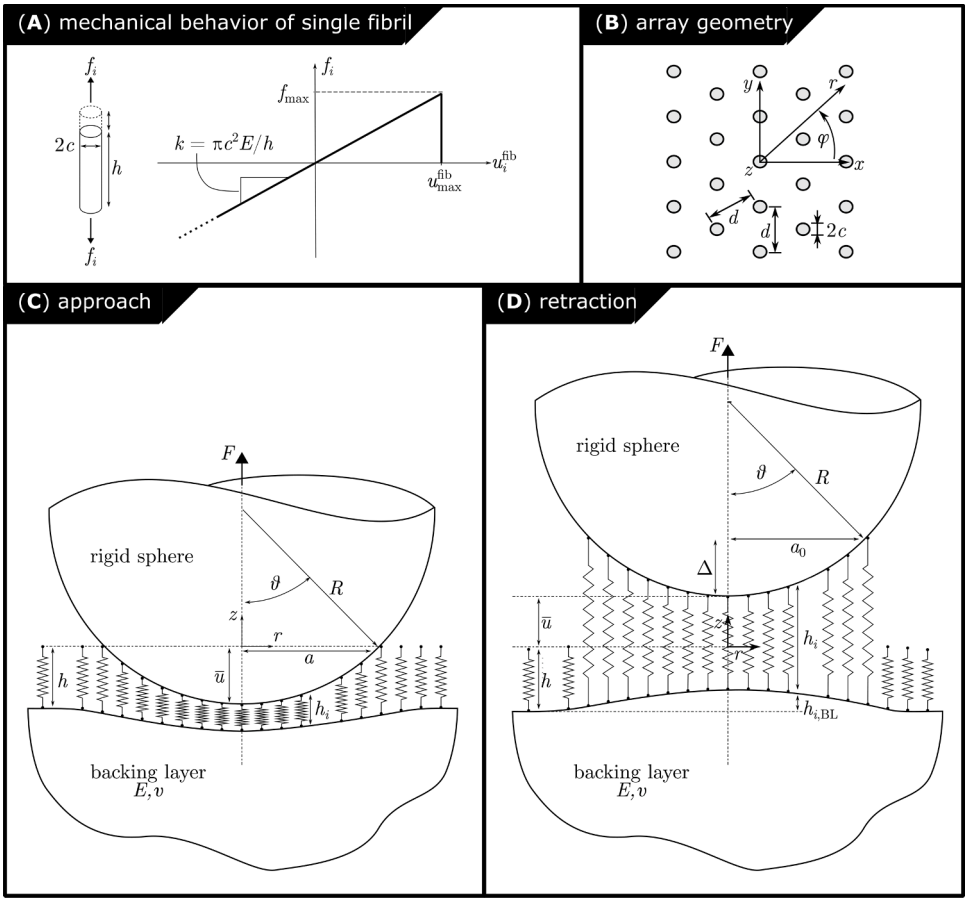


**Fig. 2.** (A) Mechanical behavior of a single fibril. It is assumed that the compressive loads experienced by fibrils are not sufficiently large to cause buckling, and that in tension the contact is maintained until a critical force $f_{\max}$ is reached. (B) Arrangement of the fibril array, showing Cartesian and polar coordinate systems. The origin of both coordinate systems is located at the center of the fibril which contacts the rigid sphere first. (C) Cross-section of the micropatterned adhesive during approach and (D) during retraction. Relevant geometric and material properties are shown in each case.

$$F_{\max} = \frac{3}{2}\pi R W_{\text{eff}}. \tag{5}$$

The JKR result is derived using approximations equivalent to linear elastic fracture mechanics, implying that significant deformation and separation of the fibrillar interface occurs in a region at the contact edge, which is very small in comparison to the dimensions of the contact itself. The elastic response must be dominated by the deformation of the backing layer. Compliance of both the backing layer and fibrils was considered by Long and Hui (2009), although only a two-dimensional plane strain continuum model is presented. This formulation does not permit a general analytical solution, however such results were obtained in various limits to augment numerical computations for non-limiting cases.

We note that a method for determining the work of adhesion that is independent of the choice of a model was proposed by Vajpayee et al. (2008) and Hui and Long (2012). Their approach requires recording of force, displacement, and contact area simultaneously in the compressive regime for loading and unloading curves. Thus, the variation in compliance with the change in contact area provides a measure of adhesion energy.

Common to all of the preceding modeling efforts is the assumption that the layer of fibrils can be modelled as continuous. In this work we seek to extend the theoretical treatment of spherical probe adhesion tests on micropatterned surfaces by considering the discrete nature of the fibrillar interface, as well as the compliance of both the fibrils and the backing layer. The results will be used to assess the validity of continuum theories for the prediction of measurement-independent estimates of the adhesive strength of fibrils in a spherical probe test configuration, and ultimately to present clear instructions for obtaining data comparable across experimental investigations.

## 2. Model

The model presented considers the micropatterned adhesive as an array of discrete one-dimensional elastic elements on an elastic backing layer, as introduced by Noderer et al. (2007), Guidoni et al. (2010), and Bacca et al. (2016).

### 2.1. General description

Fig. 2 shows a schematic representation of components of the model described. The fibrillar adhesives are modeled as a parallel array of identical, upright fibrils on an elastic backing layer (BL). The fibrils are modelled as axially loaded linear elastic cylinders with a Young's modulus of $E$, length $h$, and radius $c$. The backing layer is modeled as a linear elastic, isotropic half space of the same elastic modulus and Poisson's ratio $\nu$. The appropriateness of considering the backing layer as a half space is considered in Section 2.3.

The mechanical behavior of an individual fibril in contact is summarized in Fig. 2**A**. It is assumed that fibrils respond elastically in compression. This is considered an appropriate assumption as fibril buckling should be avoided during experimental characterization. It is readily evidenced by loss of contact at the fibril tip (Isla and Kroner, 2015; Paretkar et al., 2013). If accommodated by elastic deformation, displacement of the fibril tip relative to the point of connection to the backing layer, $u_i^{\text{fib}}$, results in a force

$$f_i = k u_i^{\text{fib}}, \tag{6}$$

where $k = \pi c^2 E/h$ is the axial stiffness of a fibril. The force $f_i$ supported by the fibril must be equilibrated by adhesive tractions at the interface between its tip and the substrate or probe. Detachment typically occurs via the propagation of a defect at this interface, with the critical load being dependent on the fibril tip geometry and defect character (Tinnemann et al., 2019b). If the variability in defect size from fibril to fibril is small, then the detachment criterion will be deterministic (Booth et al., 2019). It can be stated equivalently as a critical force $f_{\max}$, critical length $h_{\max}$, or critical elongation $u_{\max}^{\text{fib}}$. All three values are connected according to $u_{\max}^{\text{fib}} = f_{\max}/k = h_{\max} - h$.

We consider fibrils arranged in a hexagonal array as depicted in Fig. 2**B**. The number density of fibrils is $\rho = 2/(\sqrt{3}\,d^2)$. Both the Cartesian and cylindrical coordinate systems are chosen such that their origin is coincident with the center of the tip of the fibril at the array center.

Seeking to model a typical adhesion experiment, we consider the rigid spherical probe brought into contact with the array as depicted in Fig. 2**C**. The displacement of the probe $\overline{u}$ is equivalent to the $z$-position of its apex. The approach is halted when a specified indentation depth or preload condition is satisfied. The indentation depth is the absolute value of the minimum probe displacement, $\Delta = |\min(\overline{u})|$. The preload is the compressive load applied at maximum indentation, $P = |\min(F)|$.

During attachment, the interface formed by the fibril tips and the probe can be considered as an external crack that heals as the contact expands (Long and Hui, 2009). Two limits on the behavior of fibril attachment can be identified. In the first limit, contact is formed at fibril $i$ if the surface of the sphere is coincident with the fibril tip. This condition is dependent on the curvature of the probe and the applied displacement according to

$$\left(R - \sqrt{R^2 - r_i^2}\right) + \overline{u} \le 0, \tag{7}$$

where $r_i$ is the radial coordinate at the interface (see Fig. 2**B**). This condition is purely geometric, implying that adhesion does not play a role during approach and thus hysteresis is maximized. In the opposite limit, fibril $i$ may jump into contact if the associated increase in elastic strain energy is smaller than the adhesive energy gained by formation of contact with the probe at the fibril tip. The condition

is therefore

$$\Delta U_{\mathrm{el}} \leq \frac{1}{2}\frac{f_{\max}}{k^2}, \tag{8}$$

where $\Delta U_{\mathrm{el}}$ is the difference in elastic strain energy in the array. This implies that the fibril jumps into contact at the same displacement as it would detach upon retraction. There is, therefore, no hysteresis in the force-displacement curves for approach and retraction. Length scales associated with jump-into-contact on approach and detachment during separation are identified in the SI. Under the assumption that the surface interaction is dominated by short-ranged van der Waals forces, the jump-in instability is found to occur over distances of $\sim$ 10 nm while the lower bound of elongation of a fibril at detachment is found to be approximately 10 μm. This suggests that condition (7), associated with the assumption of non-adhesive approach, is an accurate approximation. We note that the presence of surface charge may cause jump-to-contact at much larger separations, thus requiring that this assumption be reconsidered.

Upon satisfaction of the preload or indentation condition, the probe is retracted as depicted in Fig. 2**D**. As the displacement $\overline{u}$ becomes positive, fibrils bear tensile load until the detachment criterion, $f_i > f_{\max}$, is satisfied.

The tip displacement of fibril $i$, if in contact, is dependent on both the probe displacement and curvature, as given by

$$u_i = \left(R - \sqrt{R^2 - r_i^2}\right) + \overline{u}. \tag{9}$$

This displacement is accommodated by deformation of both the fibril and the backing layer $u_i = u_i^{\mathrm{fib}} + u_i^{\mathrm{BL}}$. The elongation of fibril $i$ is $u_i^{\mathrm{fib}} = f_i/k = hf_i/(\pi c^2 E)$. The deformation of the backing layer is not as straightforward. The ability of this continuous layer to transmit shear dictates that it does not depend only on force transmitted to the backing layer by the fibril itself, but rather on the force transmitted by all fibrils in the array. Based on the solution for surface loading of an elastic half space (Johnson, 1985), it is determined that the force $f_j$ gives rise to deformation of the backing layer such that

$$u_i^{\mathrm{BL}}(f_j) = \frac{f_j}{\pi r_{ij} E^*}, \text{ for } j \neq i, \tag{10}$$

$$u_i^{\mathrm{BL}}(f_j) = \frac{16 f_j}{3\pi^2 c E^*}, \text{ for } j = i, \tag{11}$$

with $r_{ij}$ being the distance between centers of fibrils $i$ and $j$, and $E^* = E/(1-\nu^2)$ being the reduced Young's modulus. Eq. (10) approximates the load transmitted to the backing layer by each remote fibril, $j \neq i$, as a point contact, neglecting the dimensions of the fibril cross-section. Bacca et al. (2016) have estimated that the error associated with this approximation is within 3.5%. Eq. (11) is the average displacement of the cross-section of the fibril assuming that the load is transferred as a uniform stress.

The displacement of $i$-th fibril tip can be rewritten as

$$u_i = u_i^{\mathrm{fib}} + \sum_{j=1}^{N} u_i^{\mathrm{BL}}(f_j), \tag{12}$$

where $N$ denotes the number of fibrils in contact. Adopting summation convention for repeated indices, this equation is now formulated as a matrix product

$$u_i = c_{ij} f_j, \tag{13}$$

where $\boldsymbol{c}$ is the compliance matrix, composed of the following terms

$$c_{ij} = \frac{1}{\pi r_{ij} E^*}, \text{ for } j \neq i, \tag{14}$$

$$c_{ij} = \frac{1}{\pi c E^*}\left(\frac{16}{3\pi} + \frac{h}{c(1-\nu^2)}\right), \text{ for } j = i. \tag{15}$$

The off-diagonal terms of $\boldsymbol{c}$ encompass the mechanical coupling of fibrils by the backing layer (Bacca et al., 2016).

By defining the stiffness matrix as the inverse of the compliance matrix $\boldsymbol{k} = \boldsymbol{c}^{-1}$, it is found that $f_j = k_{ji} u_i$. The total external force is the sum of the forces on all fibrils

$$F = \sum_{i=1}^{N} f_i. \tag{16}$$

### 2.2. Numerical implementation

For numerical implementation, all equations were restated in a dimensionless form. The force supported by a single fibril was normalized by the fibril detachment force as $\widetilde{f}_i = f_i/f_{\max}$. The total force was also normalized by $f_{\max}$ as $\widetilde{F} = F/f_{\max}$ . The dimensionless

nominal stress is defined as $\widetilde{\sigma} = F/(N_0 f_{\max})$, where $N_0 = \pi a^2 \rho$ is the number of fibrils in contact at maximum indentation. This stress measure can also be interpreted as the load sharing efficiency introduced by Bacca et al. (2016). Values of $\widetilde{\sigma} < 1$ imply that at the load distribution among fibrils is non-uniform at pull-off. Displacements and distances are normalized by the fibril radius $c$, e.g. $\widetilde{u}_i = u_i / c$, with the exception of the fibril length, which we chose to define such that the normalized variable is the aspect ratio $\widetilde{h} = h/2c$. In order to simplify later equations, we introduce the dimensionless groups

$$\varepsilon_{\max} = \frac{f_{\max}}{\pi c^2 E} \text{ and } \varepsilon^*_{\max} = \frac{f_{\max}}{\pi c^2 E^*}. \tag{17}$$

The parameter $\varepsilon_{\max}$ is the strain on a fibril at detachment, thus large values indicate that the fibril is compliant and the detachment force is high. We henceforth refer to $\varepsilon^*_{\max}$ as the reduced fibril strain to detachment due to its dependence on the reduced Young's modulus, $E^*$. Note that multiplying $\varepsilon^*_{\max}$ by the reduced Young's modulus provides the adhesion strength of the fibril. Approximation of the strain to detachment for a typical fibrillar adhesive is discussed in the SI. The deformation of the backing layer, given in Eqs. (10) and (11), then is stated as

$$\widetilde{u}_i^{\mathrm{BL}}\left(\widetilde{f}_j\right) = \frac{\varepsilon^*_{\max}\widetilde{f}_j}{\widetilde{r}_{ij}}, \text{ for } j \neq i, \tag{18}$$

$$\widetilde{u}_i^{\mathrm{BL}}\left(\widetilde{f}_j\right) = \frac{16\varepsilon^*_{\max}\widetilde{f}_j}{3\pi}, \text{ for } j = i. \tag{19}$$

The dimensionless form of the compliance matrix given in Eqs. (14)–(15), is

$$\widetilde{c}_{ij} = \frac{c_{ij} f_{\max}}{c} = \frac{\varepsilon^*_{\max}}{\widetilde{r}_{ij}}, \text{ for } j \neq i, \tag{20}$$

$$\widetilde{c}_{ij} = \frac{c_{ij} f_{\max}}{c} = \varepsilon^*_{\max}\left(\frac{16}{3\pi} + \frac{2\widetilde{h}}{(1-\nu^2)}\right), \text{ for } j = i, \tag{21}$$

and the matrix product in Eq. (13) is

$$\widetilde{u}_i = \widetilde{c}_{ij}\widetilde{f}_j. \tag{22}$$

Simulations begin with the apex of the probe positioned at the origin of the coordinate system, i.e. at the tip of the central fibril. The probe is moved downwards until a specified compressive preload is reached. From this point of maximum indentation, the sphere is retracted until all fibrils detach. This was implemented computationally in Matlab (MathWorks, Natick MA, USA).

### 2.3. Experimental validation of the model

In order to validate if the model presented accurately captures the elastic response of a fibrillar array in response to approach and retraction of a spherical probe, and in particular assess the importance of consideration of backing layer compliance, we seek to compare to the results of an equivalent experiment. To do so, it is in general necessary to invoke the geometric properties of the fibril, $h$, $c$, and $d$, material properties $E$ and $\nu$, and the fibril detachment force $f_{\max}$. Of these, it is particularly difficult to obtain an a priori estimate of $f_{\max}$. In fact, the very purpose of such an experiment is to obtain a measurement-system independent adhesive strength metric such as $f_{\max}$ (see Section 1). We decide, therefore, to validate the model in the preload phase by measuring the contact area as a

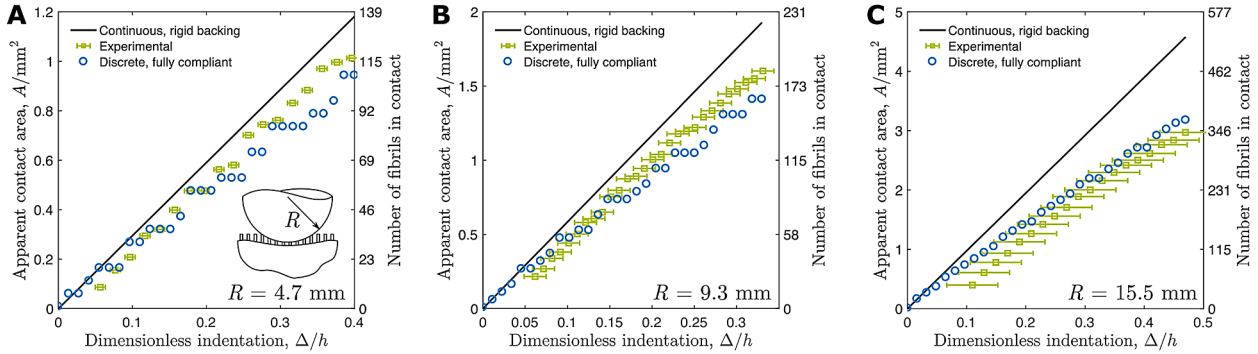


**Fig. 3.** The apparent contact area and the number of fibrils in contact as a function of dimensionless indentation depth. Results are shown for three probe radii, (A) 4.7 mm, (B), 9.3 mm, and (C) 15.5 mm. Experimental results (black circles) are compared to models assuming a rigid backing layer (green triangles) and a fully compliant backing layer (blue squares).

function of indentation depth. The results depend only on the geometry and the Poisson's ratio, for which we assume $\nu = 0.5$. No assumptions about any other material or system properties need to be considered.

For the measurements, a custom-built adhesion test setup was employed. It allowed determination of the force, the indentation depth, and the contact area in situ. The micropatterned adhesive (see Figure S1 in the SI) consisted of fibrils with a radius of 25 μm, a length of 100 μm, and a center-to-center distance of 100 μm. Fibrils were arranged hexagonally, and the backing layer was approximately 1 mm thick. The preparation of the micropatterned adhesives, the experimental procedure, and the analysis are described in the SI. The schematic of the setup is depicted in Figure S2 in the SI.

Fig. 3 shows the apparent contact area vs. the dimensionless indentation depth for the experiment, alongside both the model presented for a fully compliant backing layer and the analytical formulation for a rigid backing layer. The latter was introduced by Schargott et al. (2006) and is restated for this system in the SI. The experimental results, along with the models for both limits of backing layer compliance, demonstrate that the apparent contact area (and thus the number of fibrils in contact) monotonically increases with increasing indentation depth. Comparing the two models at a given indentation, it is observed that the compliant backing layer always yields a smaller contact. This is a consequence of backing layer deformation lowering the position of exterior fibrils, preventing the formation of contact. This effect becomes more severe as the intention depth is increased, or as the radius of the probe is increased, both of which increase the number of fibrils in contact. For the smallest spherical probe, (4.7 mm radius, Fig. 3**A**), there is not a significant difference between the models. The experimental results show good agreement with the models, independent of the assumed backing layer compliance. For larger probes (radii of 9.3 and 15.5 mm, Fig. 3**B** and **C**), there is significant difference between the two models (almost 40% for the largest sphere and the deepest indentation). The compliant limit now provides a much more accurate description of the experimental behavior. For the backing layer thickness examined, and in particular for the larger of the probe geometries considered, it is clear that compliance of the backing layer cannot be neglected.

## 3. Results

With the goal of obtaining measurement system and procedure independent estimates of adhesive strength of fibrils in mind, we begin by examining the role of preload on the behavior of spherical probe adhesion tests of the model micropatterned adhesive described in Section 2.

Fig. 4 shows the dimensionless force-displacement characteristics for approach and retraction of the probe. The fibril aspect ratio is $h/2c = 4$, the dimensionless fibril density $\pi\rho c^2 = 0.223$ (corresponding to $d/c = 4$), the dimensionless probe radius $R/c = 1000$, and the reduced fibril strain to detachment $\varepsilon^*_{\max} = 0.04$. The associated insets depict the load supported by each fibril in contact. In Fig. 4**A**, we observe that as the probe indents the adhesive, the number of fibrils in contact increases. Fibrils respond elastically in compression, as depicted in inset $\mathbf{A_1}$. With increasing indentation depth, both contact area and the compressive load increase. After the specified preload is attained, the probe is retracted. The force-displacement curve is linear up to the point at which the tensile force reaches its maximum. At this point the fibrils at the contact edge support a force close to $f_{\max}$, as evidenced in inset $\mathbf{A_2}$. Since the maximum tensile load is attained prior to the first fibril detachment, the contact area at pull-off under load control is equivalent to the contact area upon preload. Further retraction under displacement control leads to the detachment of those fibrils exceeding $f_{\max}$. The contact area shrinks from the outside in a manner comparable to an external crack propagating inward. Each fibril detachment is associated with a drop in the load, leading to a zigzagged or "saw-tooth" profile. Fig. 4**B** depicts the force-displacement characteristics of the same adhesive tested with a preload more than one order of magnitude larger than in the previous case. A fundamental difference is observed, namely

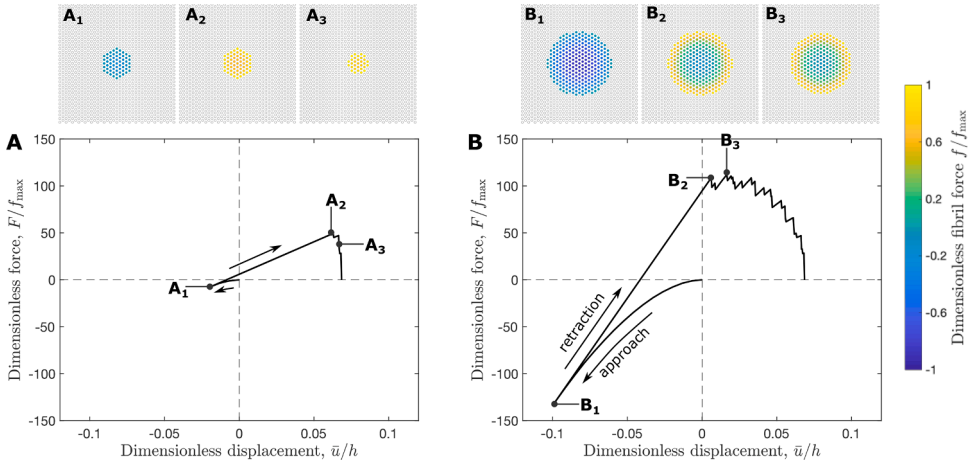


**Fig. 4.** Dimensionless force-displacement curves of a fibrillar adhesive for two values of the compressive preload, (A) $P/f_{\max} = 7.6$ and (B) $P/f_{\max} = 130$. The 2D maps above show the load distribution among the fibrils in contact. Blue indicates fibrils are in compression, whereas yellow indicates they are in tension. In (A) the first fibrils detach at the point of maximum load, whereas in (B) the first fibrils detach prior to attainment of maximum load.

that fibrils detach before the maximum load is reached. The contact area at pull-off is therefore smaller than upon preload, as shown in the insets $\mathbf{B_1}$ to $\mathbf{B_3}$. Consequently, not all fibrils initially brought into contact contribute to the pull-off force. The additional preload, required to increase the contact area above the level observed at pull-off, is therefore redundant.

Fig. 5**A** shows the pull-off force as a function of the preload for the same set of system parameters. Results are shown for both a fully compliant backing layer and a rigid backing layer. In each case the pull-off force initially increases with increasing preload, before saturating at a maximum value $F_{\max}$. Most significantly, we observe that the magnitude of the maximum pull-off force is larger for the fully compliant limit. This is a consequence of backing layer deformation at the contact edge, which reduces the load concentration in this region and delays the onset of detachment. Fig. 5**B** shows the pull-off strength versus preload. The increase in contact area under maximum preload dictates that, with increasing preload, the pull-off strength exhibits a monotonic decay due to the use of that contact area in the denominator.

In order to systematically study how the properties of the micropatterned surface control the maximum pull-off force and the onset of the saturation regime, we identify the following five dimensionless groups: the fibril aspect ratio $\widetilde{h} = h/2c$; the dimensionless fibril spacing $\widetilde{d} = d/c$ or equivalently the dimensionless fibril density $\widetilde{\rho} = \pi\rho c^2$; the dimensionless sphere radius $\widetilde{R} = R/c$; the reduced fibril strain to detachment $\varepsilon^*_{\max} = f_{\max}/(\pi c^2 E^*)$; and the Poisson's ratio $\nu$. We limit attention to cases where $\nu = 0.5$, on account of the prevalence of incompressible rubber-like materials in micropatterned adhesive fabrication (Hensel et al., 2019).

Fig. 6 shows the dependence of the pull-off force on the preload as one parameter is varied and all others are held fixed. Fig. 6**A** displays the pull-off force versus preload for four different values of the dimensionless probe radius $R/c$. It is immediately apparent that the magnitude of the maximum pull-off force increases with increasing radius, and that the onset of the saturation regime is shifted towards higher preloads. The same trend holds for increasing the dimensionless fibril aspect ratio $h/2c$ (Fig. 6**B**), fibril density $\pi\rho c^2$ (Fig. 6**C**), and fibril strain to detachment $\varepsilon^*$ (Fig. 6**D**).

In the limit of a rigid backing layer (Schargott et al., 2006) it was shown that the critical preload required to reach saturation of the pull-off force was equal to the maximum pull-off force itself, $P_{\text{crit}} = F_{\max}$. It is now revealed by inspection of Fig. 6 that the same relationship holds in the limit of the fully compliant backing layer.

Fig. 7 shows the maximum pull-off force, or equivalently the critical preload for saturation, as a function of the four dimensionless parameters describing the sphere radius $R/c$, the fibril aspect ratio $h/2c$, the fibril density $\pi\rho c^2$, and fibril strain to detachment $\varepsilon^*_{\max}$. There is a linear dependency on all parameters. It should be noted that some experimental measurements may make use of indentation depth or contact radius in place of preload. These parameters can also be computed numerically and are explored in the SI. The critical indentation depth $\Delta_{\text{crit}}/h$ increases with increasing probe radius, increasing fibril density, and increasing fibril strain to detachment. It decreases with increasing fibril length (see Figure S5). The critical contact area $a_{\text{crit}}/d$ increases with increasing probe radius, increasing fibril length, increasing fibril spacing, and increasing fibril strain to detachment (see Figure S6). Unlike the critical preload, the relationships for indentation and contact area are non-linear.

## 4. Discussion

In order to compare designs of micropatterned adhesives across experimental studies, the adhesive strength data must be independent of the measurement system and procedure. In line with this goal, the preceding results represent the first theoretical model which considers the effects of the discrete nature of the fibrillar interface, as well as both fibril and backing layer compliance, for a spherical probe test.

The first complication encountered is that the pull-off force monotonically increases with increasing preload before saturating. In preceding work considering a rigid backing layer (Schargott et al., 2006), it was shown that critical preload required to achieve saturation of the pull-off force was equal to the pull-off force itself in this regime. In this work we have shown that this condition will hold in the limit of a fully compliant backing layer and, thus, is expected to be independent of the backing layer compliance. It is

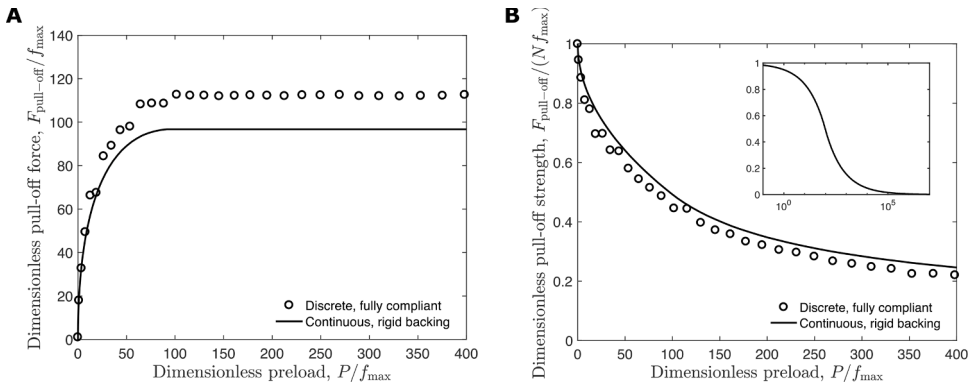


**Fig. 5.** (A) Dimensionless pull-off force and (B) pull-off strength versus dimensionless preload for the model system, where strength is defined as the pull-off force divided by the contact area at maximum preload. The inset shows that the pull-off strength converges to zero for large preloads.

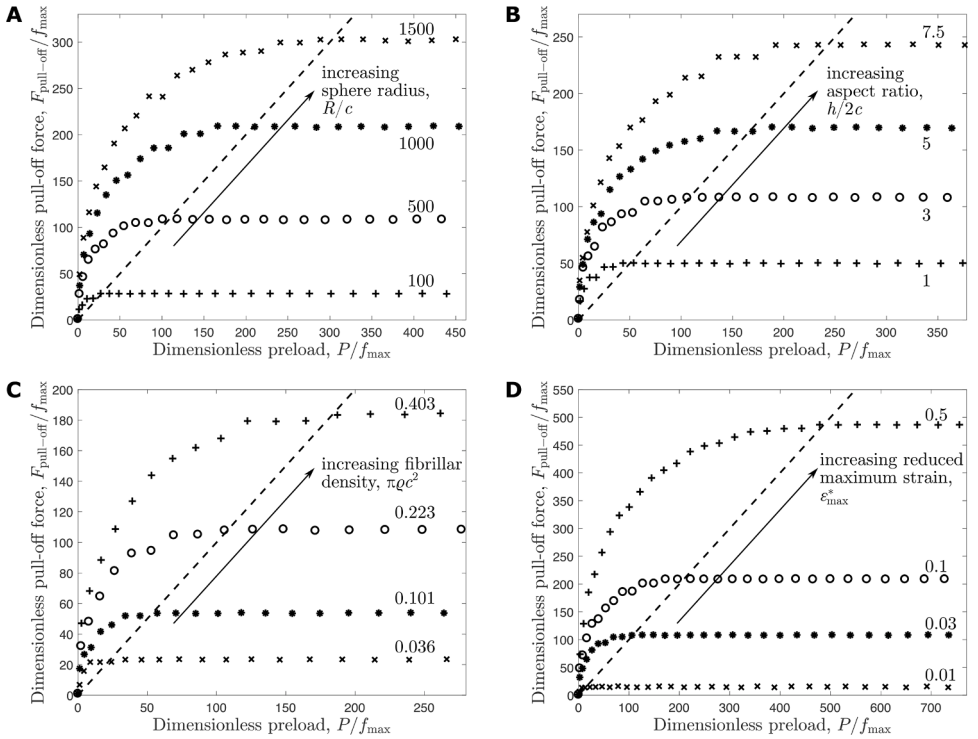


**Fig. 6.** Dimensionless pull-off force versus preload for a range of values of (A) the dimensionless sphere radius $\widetilde{R} = R/c$, (B) the aspect ratio $\widetilde{h} = h/2c$, (C) the dimensionless fibrillar density $\widetilde{\rho} = \pi\rho\mathbf{c}^2 = 2\pi\mathrm{c}^2/(\sqrt{3}\mathrm{d}^2)$, and (D) the reduced maximum strain $\varepsilon^*_{\max} = f_{\max}/(\pi c^2 E^*)$. In each case the highlighted parameter was varied while other parameters remained constant in the standard configuration of $R/c = 500$, $h/2c = 3$, $\pi\rho\mathrm{c}^2 = 0.223$, and $\varepsilon^*_{\max} = f_{\max}/(\pi c^2 E^*) = 0.1$. The dashed lines have a gradient of 1, and mark the onset of the saturation regime.

therefore essential that measurements are performed with increasing preload until saturation is observed. It should additionally be ensured that this saturation is not associated with full contact of all fibrils in the array, as the resulting force would then additionally be a property of the array size.

Saturation of the pull-off force is, however, insufficient to ensure that the results are independent of the properties of the measurement system and procedure. This work has also revealed a dependency of the pull-off force on the compliance of the backing layer through the two limiting cases examined. Models capable of extracting an objective measure of strength, including the one presented in this paper, exclusively consider the limits of a rigid or fully compliant (elastic half-space) backing layer on account of the lack of a closed-form solution for a finite thickness domain subject to normal loading. It may be possible to modify the backing layer compliance terms using a semi-empirical correction factor, such as is presented in Long et al. (2008), to account for finite backing layer thickness. However, in addition to avoiding reliance on this approximate solution, it is recommended that operation in the fully compliant limit be ensured in experiment for the following reason. Typical micropatterned adhesives are fabricated on a backing layer of the same component material, with specified thickness. It is more difficult to repeatably fabricate a backing layer which is very thin, and thus behaves as rigid on account of the surface to which it is mounted. The backing layer thickness should ideally be increased until an effect on the maximum pull-off force is no longer observed. In this work, a thickness one order of magnitude larger than the fibril height was seen to be sufficient to operate in the fully compliant limit (Section 2.3), although this will depend on the specific fibril and array properties under consideration.

The final dependency to be considered is on the probe radius. In Section 1, continuum theories were introduced which describe this dependency and, in theory, allow for the extraction of an objective measure of strength. The limit represented by DMT theory (or equivalently the model of Schargott for a fibrillar interface) is associated with domination of fibril deformation when compared to the backing layer. The limit represented by JKR theory implies that deformation of the backing layer is dominant, as linear elastic fracture mechanics requires deformation and separation of the interface occurs in a region (termed the 'fracture process zone') which is very small in comparison to the dimensions of the contact. The validity of this assumption can be assessed by comparing estimates of the lateral extent of the fracture process zone to the critical contact radius, or equivalently using the parameter introduced by Tabor (Tabor, 1977). The latter can be stated in terms of the system parameters as

$$\mu = \left(\frac{\widetilde{\rho}^2\widetilde{R}\varepsilon_{\max}}{4\widetilde{h}}\right)^{\frac{1}{3}}, \tag{23}$$

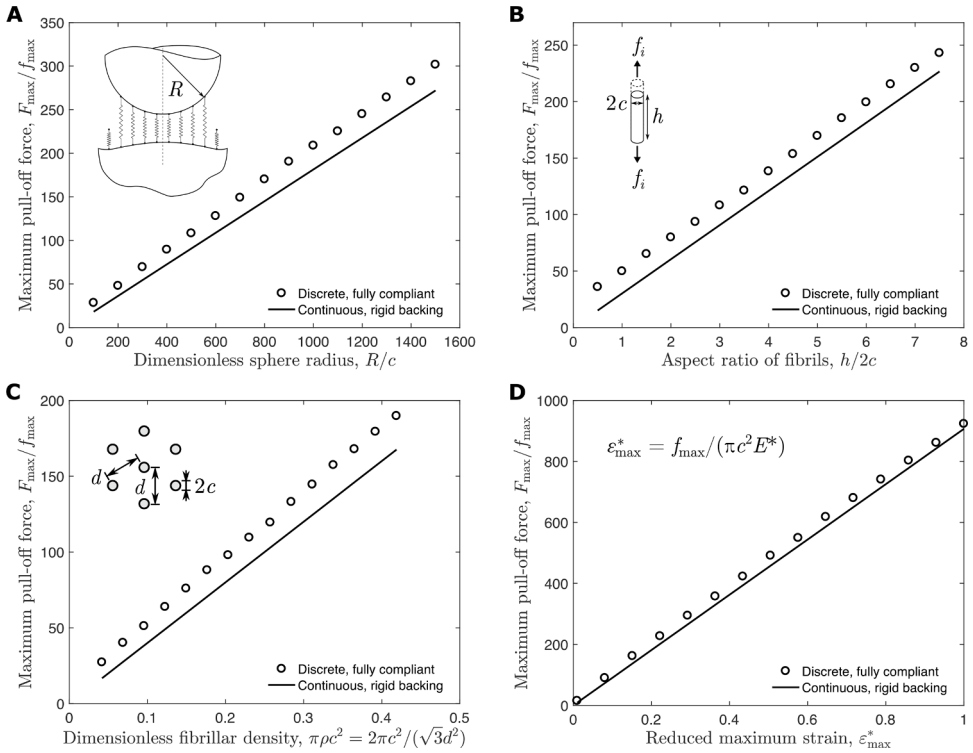


**Fig. 7.** Dimensionless maximum pull-off force $F_{max}/f_{max}$, or critical preload $P_{crit}/f_{max}$ for a range of values of (A) the dimensionless sphere radius $\widetilde{R} = R/c$, (B) the aspect ratio $\widetilde{h} = h/2c$, (C) the dimensionless fibrillar density $\widetilde{\rho} = \pi\rho c^2 = 2\pi c^2/(\sqrt{3}d^2)$, and (D) the reduced fibril strain to detachment $\varepsilon^*_{max} = f_{max}/(\pi c^2 E^*)$. In all cases the critical preload is approximately equal to the maximum pull-off force. In each case the highlighted parameter was varied while all other parameters remained constant in the standard configuration of $R/c = 500$, $h/2c = 3$, $\pi\rho c^2 = 0.223$ (corresponding to $d/c = 4$), and $\varepsilon^*_{max} = f_{max}/(\pi c^2 E^*) = 0.1$. Each data point corresponds to one pull-off force versus preload curve, as shown in Fig. 6. Solid lines show the solution for a rigid backing layer. Note that the scales on the y-axis are not uniform across the plots.

where validity of the JKR theory requires $\mu > 5$, and validity of the DMT theory requires $\mu < 0.1$.

We seek to compare the results of the discrete model to these continuum theories by normalizing the results of Fig. 7 as $F_{max}/\pi R W_{eff}$, which is calculated from the dimensionless system parameters according to

$$\frac{F_{max}}{\pi R W_{eff}} = \frac{\widetilde{F}_{max}}{\widetilde{R}\widetilde{h}\widetilde{\rho}\varepsilon_{max}}. \tag{24}$$

Fig. 8 shows the maximum pull-off force normalized as $F_{max}/\pi R W_{eff}$, as a function of the four dimensionless system parameters highlighted in the preceding section. Additionally, it shows the variation in the Tabor parameter as a function of these parameters. The results of the discrete model, in both the limit of a fully compliant and a rigid backing layer, are shown alongside the predictions of continuum JKR and DMT theories.

In general, we observe that the Tabor parameter suggests that the results should fall in an intermediate regime, closer to the DMT limit, across the majority of the parameter space. However, the predictions of the normalized detachment force from the discrete model, in either limit of backing layer compliance, do not sit between the lower bound of the JKR theory and the upper bound of the DMT theory. Instead, they are consistently higher than both. The result of the DMT and Schargott models is only asymptotically approached for large probe radii and for fibrils which are compliant relative to the backing layer. The absence of a transition between the continuum theory results according to the Tabor parameter, suggests that the discrete nature of the interface plays a dominant role in the response of micropatterned adhesives as system parameters are varied in a typical spherical probe adhesion test.

The dominance of discretization effects ultimately dictate that a discrete simulation should accompany each experimental spherical probe adhesion test, in order to extract an objective measure of the fibril adhesive strength. Accordingly, the numerical model utilized in this work has been adapted into a convenient tool for use by experimentalists. The user provides the geometric parameters of their system (fibrils, array, and probe), the elastic properties of the component material, and the measured saturation pull-off force on a fully-compliant backing layer. Given that the model requires a priori specification of the fibril strength, specifically the fibril strain to detachment $\varepsilon_{max}$, this parameter must be incrementally varied until a solution corresponding to the users specified pull-off force is obtained. The corresponding value of $\varepsilon_{max}$ represents a measure of strength suitable for comparison across experimental investigations. Alternative measures of strength are also provided, namely the fibril detachment force, $f_{max}$, and effective work of adhesion, $W_{eff}$. Matlab code for the main script ('SphericalProbe_ExtractFibrilStrength.m') and associated functions is available online (https://

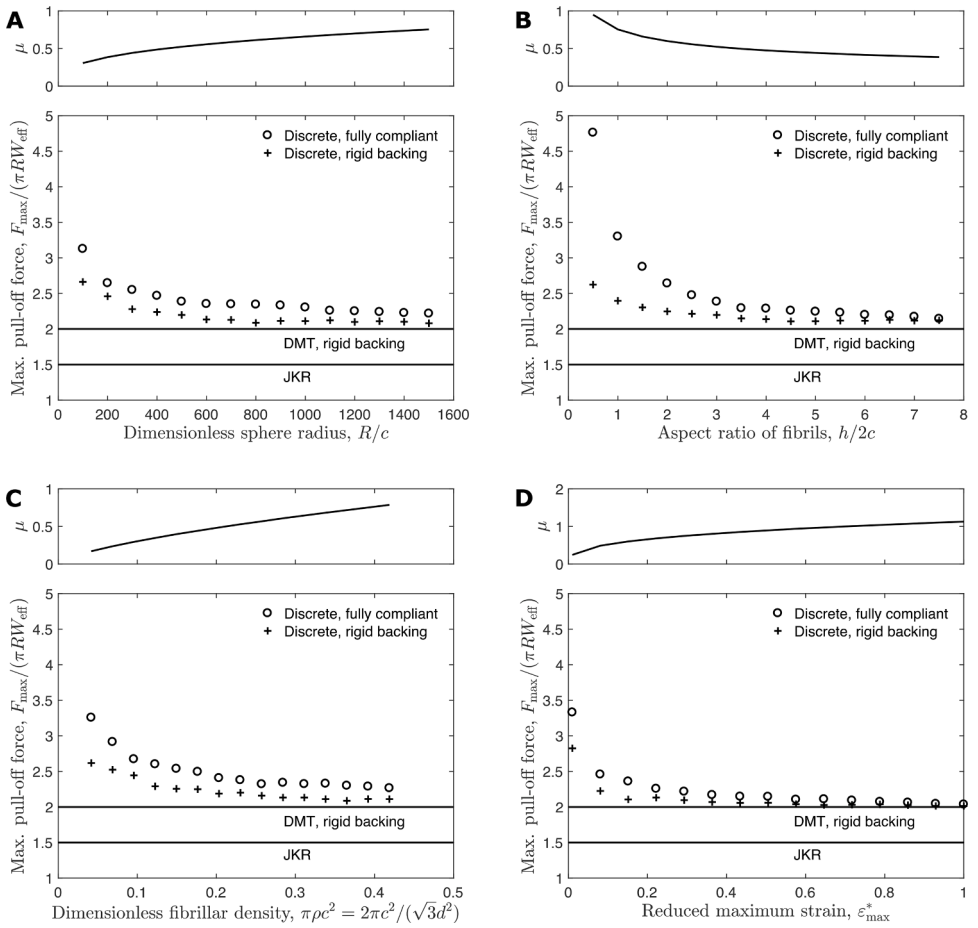


**Fig. 8.** Normalized maximum pull-off force, $F_{max}/\pi RW_{eff}$, and the Tabor parameter, $\mu$, versus (A) the dimensionless sphere radius $\widetilde{R} = R/c$, (B) the aspect ratio $\widetilde{h} = h/2c$, (C) the dimensionless fibrillar density $\widetilde{\rho} = \pi\rho c^2 = 2\pi c^2/(\sqrt{3}\,d^2)$, and (D) the reduced maximum strain $\varepsilon^*_{max} = f_{max}/(\pi c^2 E^*)$. In each case the highlighted parameter was varied while all other parameters remained constant in the standard configuration of $R/c = 500$, $h/2c = 3$, $\pi\rho c^2 = 0.223$ (corresponding to $d/c = 4$), and $\varepsilon^*_{max} = f_{max}/(\pi c^2 E^*) = 0.1$. The predictions of DMT and JKR theories are also shown.

github.com/jamieabooth/sphericalprobe). This approach has been used in conjunction with the experimental data presented in Fig. 1, as well as on a second data set associated with a different fibril and array geometry presented in Figure S7 of the SI. For the first adhesive, with 25 μm radius fibrils, fibril strain to detachment extracted by the model is found to be 0.0832, 0.0909, and 0.104 for probe radii 4.7 mm, 9.3 mm, and 15.5 mm, respectively. Multiplying these values by the reduced Young's modulus of PDMS of 2.66 MPa results in the fibril adhesive strength of $0.24 \pm 0.02$ MPa (see eq. (17)). For the second adhesive, with 3.5 μm radius fibrils, the deviation in the strength across all probe radii is smaller. Fibril strain to detachments extracted by the model are 0.164, 0.170, and 0.163, respectively. Therefore, the fibril adhesive strength is $0.44 \pm 0.01$ MPa. This result demonstrates that smaller fibrils create larger adhesion in accordance with previous reports, e.g. (Hensel et al., 2018).

## 5. Conclusions

The aim of the present study is to extend previous theoretical treatments of spherical probe tests of micropatterned adhesives by considering both the role of backing layer compliance and discretization of the contact. The ultimate goal of any adhesion test is to extract a performance metric which is independent of the properties of the measurement system and procedure. Across a range of system parameters relevant to the characterization of state-of-the-art synthetic micropatterned adhesives, it is observed that the effect of discretization of the contact is dominant and the predictions of continuum theories break down. Accordingly, it is concluded that a discrete simulation should accompany each experimental test in order to extract an objective measure of fibril strength. Tests should be performed to the point of saturation of the pull-off force with increasing preload, using a compliant backing layer of the same component material. The measured maximum pull-off force can be inputted in to the numerical tool (https://github.com/jamieabooth/sphericalprobe) provided for discrete simulation in order to extract an objective measure of the fibril adhesive strength.

## CRediT authorship contribution statement

**Simon Bettscheider:** Methodology, Software, Investigation, Writing – original draft. **Dan Yu:** Investigation, Resources. **Kimberly L. Foster:** Conceptualization, Supervision, Writing – review & editing. **Robert M. McMeeking:** Conceptualization, Supervision, Writing – review & editing. **Eduard Arzt:** Conceptualization, Supervision, Funding acquisition. **René Hensel:** Conceptualization, Supervision, Writing – review & editing. **Jamie A. Booth:** Conceptualization, Supervision, Methodology, Software, Investigation, Writing – review & editing.

## Declaration of Competing Interest

The authors declare that they have no known competing financial interests or personal relationships that could have appeared to influence the work reported in this paper.

## Acknowledgments

SB, DY, EA, and RH acknowledge funding from the European Research Council (ERC) under the European Union's Seventh Framework Program (FP/2007–2013)/ERC Advanced Grant No. 340929. RMM acknowledges the Alexander von Humboldt Foundation for awarding the "Virtual Humboldt Cluster on the Mechanics and Physics of Adhesion and Grip".

## Supplementary materials

Supplementary material associated with this article can be found, in the online version, at doi:10.1016/j.jmps.2021.104365.

## References

Bacca, M., Booth, J.A., Turner, K.L., McMeeking, R.M., 2016. Load sharing in bioinspired fibrillar adhesives with backing layer interactions and interfacial misalignment. J. Mech. Phys. Solids 96, 428–444. https://doi.org/10.1016/j.jmps.2016.04.008.

Barreau, V., Yu, D., Hensel, R., Arzt, E., 2017. Elevated temperature adhesion of bioinspired polymeric micropatterns to glass. J. Mech. Behav. Biomed. Mater. 76, 110–118. https://doi.org/10.1016/j.jmbbm.2017.04.007.

Booth, J.A., Bacca, M., McMeeking, R.M., Foster, K.L., 2018. Benefit of backing-layer compliance in fibrillar adhesive patches-resistance to peel propagation in the presence of interfacial misalignment. Adv. Mater. Interfaces 5, 1800272. https://doi.org/10.1002/admi.201800272.

Booth, J.A., Tinnemann, V., Hensel, R., Arzt, E., McMeeking, R.M., Foster, K.L., 2019. Statistical properties of defect-dependent detachment strength in bioinspired dry adhesives. J. R. Soc. Interface 16, 20190239. https://doi.org/10.1098/rsif.2019.0239.

Cheung, E., Sitti, M., 2009. Adhesion of biologically inspired polymer microfibers on soft surfaces. Langmuir 25, 6613–6616. https://doi.org/10.1021/la900997p.

Derjaguin, B., Muller, V., Toporov, Y., 1975. Effect of contact deformations on the adhesion of particles. J. Colloid Interface Sci. 53, 314–326. https://doi.org/10.1016/0021-9797(75)90018-1.

Greiner, C., Buhl, S., Campo, A.del, Arzt, E., 2009. Experimental parameters controlling adhesion of biomimetic fibrillar surfaces. J. Adhes. 85, 646–661. https://doi.org/10.1080/00218460902997042.

Greiner, C., del Campo, A., Arzt, E., 2007. Adhesion of bioinspired micropatterned surfaces: effects of pillar radius, aspect ratio, and preload. Langmuir 23, 3495–3502. https://doi.org/10.1021/la0633987.

Guidoni, G.M., Schillo, D., Hangen, U., Castellanos, G., Arzt, E., McMeeking, R.M., Bennewitz, R., 2010. Discrete contact mechanics of a fibrillar surface with backing layer interactions. J. Mech. Phys. Solids 58, 1571–1581. https://doi.org/10.1016/j.jmps.2010.07.009.

Hensel, R., McMeeking, R.M., Kossa, A., 2019. Adhesion of a rigid punch to a confined elastic layer revisited. J. Adhes. 95, 44–63. https://doi.org/10.1080/00218464.2017.1381603.

Hensel, R., Moh, K., Arzt, E., 2018. Engineering micropatterned dry adhesives: from contact theory to handling applications. Adv. Funct. Mater. 28, 1800865 https://doi.org/10.1002/adfm.201800865.

Hui, C.-.Y., Long, R., 2012. Direct extraction of work of adhesion from contact experiments: generalization of JKR theory to flexible structures and large deformation. J. Adhes. 88, 70–85. https://doi.org/10.1080/00218464.2011.611090.

Isla, P.Y., Kroner, E., 2015. A novel bioinspired switchable adhesive with three distinct adhesive states. Adv. Funct. Mater. 25, 2444–2450. https://doi.org/10.1002/adfm.201500241.

Jagota, A., 2002. Mechanics of adhesion through a fibrillar microstructure. Integr. Comp. Biol. 42, 1140–1145. https://doi.org/10.1093/icb/42.6.1140.

Johnson, K.L., 1985. Contact Mechanics. Cambridge University Press, Cambridge. https://doi.org/10.1017/CBO9781139171731.

Johnson, K.L., Kendall, K., Roberts, A.D., 1971. Surface energy and the contact of elastic solids. Proc. R. Soc. A Math. Phys. Eng. Sci. 324, 301–313. https://doi.org/10.1098/rspa.1971.0141.

Khaled, W.Bin, Sameoto, D., 2013. Anisotropic dry adhesive via cap defects. Bioinspir. Biomim. 8, 044002 https://doi.org/10.1088/1748-3182/8/4/044002.

Kroner, E., Paretkar, D.R., McMeeking, R.M., Arzt, E., 2011. Adhesion of flat and structured PDMS samples to spherical and flat probes: a comparative study. J. Adhes. 87, 447–465. https://doi.org/10.1080/00218464.2011.575317.

Long, R., Hui, C.-.Y., 2009. The effect of preload on the pull-off force in indentation tests of microfibre arrays. Proc. R. Soc. A Math. Phys. Eng. Sci. 465, 961–981. https://doi.org/10.1098/rspa.2008.0362.

Long, R., Hui, C.Y., Kim, S., Sitti, M., 2008. Modeling the soft backing layer thickness effect on adhesion of elastic microfiber arrays. J. Appl. Phys. 104, 1–9. https://doi.org/10.1063/1.2968249.

Mengüç, Y., Yang, S.Y., Kim, S., Rogers, J.A., Sitti, M., 2012. Gecko-inspired controllable adhesive structures applied to micromanipulation. Adv. Funct. Mater. 22, 1246–1254. https://doi.org/10.1002/adfm.201101783.

Minsky, H.K., Turner, K.T., 2017. Composite microposts with high dry adhesion strength. ACS Appl. Mater. Interfaces 9, 18322–18327. https://doi.org/10.1021/acsami.7b01491.

Noderer, W.L., Shen, L., Vajpayee, S., Glassmaker, N.J., Jagota, A., Hui, C.-.Y., 2007. Enhanced adhesion and compliance of film-terminated fibrillar surfaces. Proc. R. Soc. A Math. Phys. Eng. Sci. 463, 2631–2654. https://doi.org/10.1098/rspa.2007.1891.

Paretkar, D., Kamperman, M., Martina, D., Zhao, J., Creton, C., Lindner, A., Jagota, A., McMeeking, R., Arzt, E., 2013. Preload-responsive adhesion: effects of aspect ratio, tip shape and alignment. J. R. Soc. Interface 10, 20130171. https://doi.org/10.1098/rsif.2013.0171. –20130171.

Schargott, M., Popov, V.L., Gorb, S., 2006. Spring model of biological attachment pads. J. Theor. Biol. 243, 48–53. https://doi.org/10.1016/j.jtbi.2006.05.023.
Tabor, D., 1977. Surface forces and surface interactions. J. Colloid Interface Sci. 58, 2–13. https://doi.org/10.1016/0021-9797(77)90366-6.
Tinnemann, V., Arzt, E., Hensel, R., 2019a. Switchable double-sided micropatterned adhesives for selective fixation and detachment. J. Mech. Phys. Solids 123, 20–27. https://doi.org/10.1016/j.jmps.2018.09.003.
Tinnemann, V., Hernández, L., Fischer, S.C.L., Arzt, E., Bennewitz, R., Hensel, R., 2019b. In situ observation reveals local detachment mechanisms and suction effects in micropatterned adhesives. Adv. Funct. Mater., 1807713 https://doi.org/10.1002/adfm.201807713.
Vajpayee, S., Hui, C.-Y., Jagota, A., 2008. Model-independent extraction of adhesion energy from indentation experiments. Langmuir 24, 9401–9409. https://doi.org/10.1021/la800817x.
Yu, D., Beckelmann, D., Opsölder, M., Schäfer, B., Moh, K., Hensel, R., de Oliveira, P., Arzt, E., 2018. Roll-to-roll manufacturing of micropatterned adhesives by template compression. Materials (Basel) 12, 97. https://doi.org/10.3390/ma12010097.